forum acusticum 2026
8-12 September · Graz, Austria

DEVELOPING A MEASUREMENT SYSTEM TO DETERMINE HUMAN EAR CANAL WALL MECHANICAL IMPEDANCE IN-SITU: EFFECT AND SUPPRESSION OF TORSIONAL MOTIONS IN THE PROTOTYPE

Marius Benkert[1], Erwin Kuipers[2], Matthias Blau[1,3]

[1] *Jade University of Applied Sciences, Germany*
[2] *Sonova AG, Switzerland*
[3] *Cluster of Excellence Hearing4All*

Abstract

When wearing hearing aids, a mechanical interaction between the earmould and the skin of the outer ear canal occurs. The extent of this interaction, its influence on wearing comfort and long-term effects caused by continuously wearing a hearing aid are largely unknown. To quantify this interaction we develop a measurement system to measure the mechanical point impedance inside the human ear canal. The measurement system consists of an acceleration sensor and a vibration exciter that are both mounted on a cantilever beam. An electromechanically motivated model is used to estimate the attached mechanical load impedance. Because the model neglects torsional motion, a finite-element (FE) model of the device was used to evaluate the induced rotational velocity for ideal and misaligned sensor/actuator placements. Furthermore, a tuning-fork-shaped beam was investigated in the simulation as a means to suppress torsional components. The FE analysis shows that the tuning-fork geometry reduces rotational velocity compared to a conventional rectangular beam. Prototypes incorporating the new beam were subsequently built and analyzed using Laser-Doppler-Vibrometry, indicating a modest reduction in torsional motion for the new design.

Keywords: *ear canal, mechanical impedance, electromechanical model, torsion*

Corresponding author: *marius.benkert[at]jade-hs.de.*

1. Introduction

The measurement of mechanical impedances usually incorporates a dynamic force sensor and a velocity sensor. Due to the lack of available space inside the ear canal, we developed a measurement system consisting of a vibration exciter and an acceleration sensor that are both mounted on a cantilever beam.

The attached mechanical load impedance is estimated by utilizing the transfer function between acceleration sensor signal and input voltage to the exciter. This transfer function reflects the mechanical behavior of the measurement system and it changes when a load is attached. Furthermore, a relationship between the measured transfer function and the attached load impedances can be established. The underlying model is described in section 2.

The model is one dimensional and assumes only translational motion. Since rotations are not part of the underlying calibration model, we assumed that it could negatively influence the estimation accuracy of the measurement device. In this paper, we investigate beam torsion as a potential source of error. We quantify the magnitude of torsional motion and assess its influence on the accuracy of the mechanical load impedance estimation.

Before addressing this question, the following section briefly introduces the calibration and estimation approach and outlines the underlying mathematical framework.

2. Measurement principle

The measurement principle is described in detail in [1] and is briefly summarized here. The mechanical load impedance is estimated through

$$Z_{\mathrm{mech,est}} = \frac{H_{\mathrm{meas}}^{-1} - a_{11}}{a_{12}} \tag{1}$$

where a_{11} and a_{12} are the model parameters and H_{meas}^{-1} is the inverse measured transfer function

$$H_{\text{meas}}^{-1} = \frac{u}{a} \tag{2}$$

with the exciter input voltage u and the measured acceleration a at the tip of the measurement device. To obtain the parameters a_{11} and a_{12}, a system of equations with N ($N \geq 2$) measurements of transfer functions H_n^{-1} with known load impedances $Z_{L,n}$ can be arranged as

$$\begin{bmatrix} H_{L,1}^{-1}(\omega) \\ H_{L,2}^{-1}(\omega) \\ \vdots \\ H_{L,N}^{-1}(\omega) \end{bmatrix} = \begin{bmatrix} 1 & Z_{L,1}(\omega) \\ 1 & Z_{L,2}(\omega) \\ \vdots & \vdots \\ 1 & Z_{L,N}(\omega) \end{bmatrix} \begin{bmatrix} a_{11}(\omega) \\ a_{12}(\omega) \end{bmatrix}. \tag{3}$$

This system of equations can be solved in the least squares sense.

3. Measurement probe designs

This paper investigates torsional motion in two probe designs. The chosen designs are shown in Figure 1.

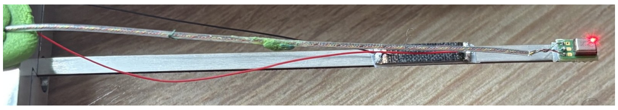

(a) Rectangular beam

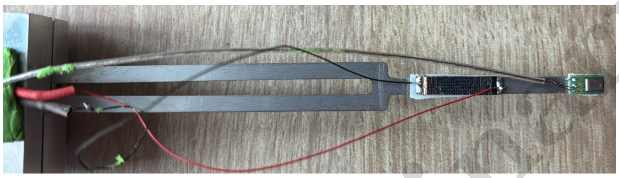

(b) Tuning-fork-shaped beam

Figure 1: Physical prototypes of the measurement device with (a) a rectangular beam and (b) a tuning-fork-shaped beam.

Figure 1 (a) shows a rectangular cantilever beam with length $l = 90\,\text{mm}$, width $w = 3\,\text{mm}$ and height $h = 0.5\,\text{mm}$. Figure 1 (b) shows a tuning-fork-shaped cantilever beam with total length of $l = 103\,\text{mm}$, width $w = 3\,\text{mm}$ and height $h = 0.5\,\text{mm}$. The legs are 40 mm long and separated by 3 mm. The 30 mm long front section is connected to the legs by a 3 mm long and 9 mm wide crosspiece. The tuning-fork-shaped beam was designed to reduce torsional motion while largely preserving translational motion. The torsional stiffness of a rectangular beam is proportional to width w^3 and height h, while the bending stiffness is proportional to w and h^3 [2, p.18, 24]. Thus, increasing the effective beam width, as implemented in the tuning-fork-shaped design, increases torsional stiffness more strongly than bending stiffness.

4. Finite-element analysis of translational and torsional probe tip motion

The motion of the measurement device was simulated using a three-dimensional FE model in COMSOL (version 6.3). The simulations were performed using the Solid Mechanics module. The 3D model of both beam designs is shown in Figure 2.

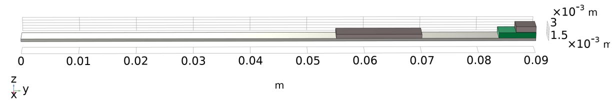

(a) Rectangular beam

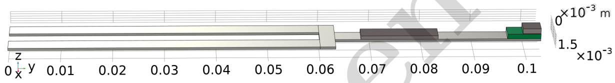

(b) Tuning-fork-shaped beam

Figure 2: COMSOL model of measurement device with (a) rectangular beam and (b) tuning-fork-shaped beam.

The beams were modeled as steel AISI 4340. Structural damping was included by adding a loss factor $\eta = 0.01$ to the Young's Modulus E as $E' = E(1 + j\eta)$ [2, p.59]. The acceleration sensor was modeled using FR4 for the circuit board and nickel for the sensor housing, with material parameters taken from the COMSOL material library. For the piezoelectric actuator, lead zirconate titanate was used as the base material, with the material parameters specified according to manufacturer data to $\rho_{\text{piezo}} = 2400\,\text{kg/m}^3$, $E_{\text{piezo}} = 70\,\text{GPa}$ and $\nu_{\text{piezo}} = 0.3$.
The beam is clamped at $y = 0\,\text{m}$ and free otherwise. A frequency-independent boundary load of $F_0 = 1\,\text{mN}$ was applied at the contact surface between the piezoelectric exciter and the beam. Offsets in the x-direction were introduced for the piezoelectric exciter and the acceleration sensor to represent realistic assembly asymmetries. A physics-controlled mesh of triangles with normal element size was generated. At the highest investigated frequency of 6 kHz, the mesh resolution corresponded to at least six elements per wavelength [2, pp.469].

4.1. Method

The expected motion of the probe tip is shown in Figure 3. For the current paper we investigate rotations around the y-axis and translations along the z-axis. Due to bending waves in the beam, rotation about the x-axis may also occur. This motion and its influence on estimation accuracy are not considered in the present paper.
Translational motion along the x-axis is neglected here because its influence on the velocity in z-direction is negligible. The same applies to rotations around the z-axis.
The overall velocity in z-direction v_{avrg} was obtained

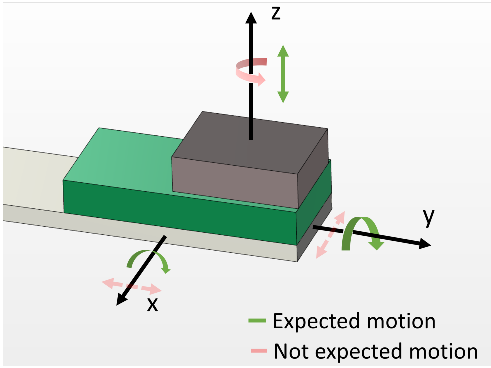

Figure 3: Expected (green) and neglected (red) degrees of freedom for the probe tip.

by averaging the velocity over the top surface area of the acceleration sensor. This approximation is intended to represent the spatial averaging performed by the physical sensor

In order to provide a link to velocity measurements and to better estimate the introduced error through the occurrence of rotation, we use the tangential velocity to characterize the rotation rather than the angular velocity. Because the sensor is mainly measuring the z-component of the velocity, we will focus on the z-component $v_{\mathrm{z,rot}}$ of the tangential velocity. To obtain $v_{\mathrm{z,rot}}$ we can measure the complex valued velocity at the edges of the probe tip and then calculate $v_{\mathrm{z,rot}}$ as

$$v_{\mathrm{z,left,total}} = v_{\mathrm{transl.}} + v_{\mathrm{z,rot}} \tag{4}$$

$$v_{\mathrm{z,right,total}} = v_{\mathrm{transl.}} - v_{\mathrm{z,rot}} \tag{5}$$

$$v_{\mathrm{z,rot}} = \frac{1}{2}(v_{\mathrm{z,left,total}} - v_{\mathrm{z,right,total}}) \tag{6}$$

This works because of the phase difference in $v_{\mathrm{z,rot}}$ between left and right side.

4.2. Simulation results

Figure 4 shows the velocities in z-direction for both beam designs for offsets of the acceleration sensor ranging from 0 mm to 0.5 mm in 0.1 mm steps.

If all components are positioned on the centerline of the beam, the rotational contribution to the z-direction velocity is negligible. However, when the acceleration sensor is positioned off-center, the rotation-induced z-direction velocity approaches the translational velocity with increasing frequency.

The average level difference between the average translational velocity and the rotation-induced part is around 65 dB for the tuning-fork-shaped beam while it is 63 dB for the rectangular beam. The average level difference for frequencies above 1000 Hz is 29 dB for the tuning-fork-shaped beam and 25 dB for the rectangular beam. Smaller level differences indicate a larger relative contribution of rotational motion. Thus, the tuning-fork-shaped beam provides a small benefit over the rectangular beam.

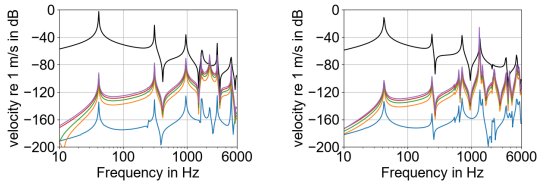

(a) Rectangular beam (b) Tuning-fork-shaped beam

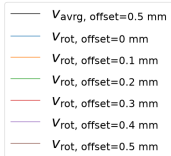

Figure 4: Velocity components for various off center positions of the acceleration sensor for (a) the rectangular beam and (b) the tuning-fork-shaped beam.

5. Measurements of probe tip motion

The previous sections showed that the expected rotational motions are relatively small. In order to characterize the influence of beam torsion in practice, we can reformulate (4) to (6) by multiplying both sides of equations (4) to (6) by the inverse input voltage $1/u_{\mathrm{in}}$. This yields

$$H_{\mathrm{z,rot}} = \frac{1}{2}(H_{\mathrm{z,left,total}} - H_{\mathrm{z,right,total}}) \tag{7}$$

with

$$H_{\mathrm{z,left/right,total}} = \frac{v_{\mathrm{z,left/right,total}}}{u_{\mathrm{in}}} \tag{8}$$

$$H_{\mathrm{z,rot}} = \frac{v_{\mathrm{z,rot}}}{u_{\mathrm{in}}}. \tag{9}$$

5.1. Measurement setup

The measurements were performed using a laser Doppler vibrometer (Polytec type CLV-700, *https://www.polytec.com*) connected to a multi-channel audio interface (RME Fireface UC, *https://rme-audio.com/home.html*) operating at a sampling rate of $f_{\mathrm{s}} = 48\,\mathrm{kHz}$. The measurement was controlled via a custom audio measurement software (*https://gitlab.gwdg.de/marius.benkert02/cheesecake*). The measurement probe consisted of a piezo vibration exciter (FLORA innovations, Dragonfly, *https://flora.tech*), an acceleration sensor (PUIAudio, VMM-1627L-R, *https://puiaudio.com*) and laser-cut stainless-steel beams as specified in section 3.

5.2. Measurement results

Figure 5 shows the resulting transfer functions for translational and rotational motions for both beam designs. The corresponding level difference between the translational and rotational transfer functions is shown in Figure 5 (c). To obtain the total velocity in z-direction, the acceleration sensor was first calibrated using a HBK shaker (Type 4810) and the laser vibrometer. For this, the acceleration sensor was placed on the shaker. The velocity at the center of the sensor was measured using the laser vibrometer positioned above the sensor. The transfer function

$$H_{\mathrm{laser/acc}} = \frac{v_{\mathrm{laser}}}{u_{\mathrm{acc}}} \tag{10}$$

defined as the ratio between the velocity v_{laser} measured by the laser vibrometer and the voltage u_{acc} obtained from the acceleration sensor, was used to calibrate the acceleration sensor.
Between 100 Hz and 6 kHz, the magnitude-squared coherence (MSC) was close to one. Below 100 Hz, the MSC was too low for a reliable analysis.

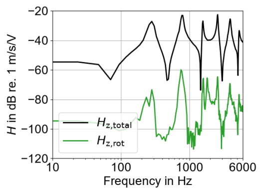

(a) Rectangular Beam

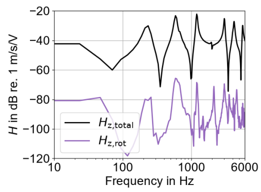

(b) Tuning-fork-shaped beam

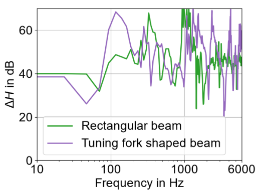

(c) Level difference between translation and rotation

Figure 5: Measured translational and rotational motion for (a) the rectangular beam and (b) the tuning-fork-shaped beam. (c) shows the level differences between translational and rotational motion for both beam designs.

Consistent with the simulations, the level difference between $H_{\mathrm{z,rot}}$ and H_{total} is large for low frequencies. Contrary to the simulation results, the measured rotational contribution did not increase with frequency. The average level difference between translational and torsional motion was 38 dB for the rectangular beam and 39 dB for the tuning-fork-shaped beam. Above 1 kHz, the corresponding level differences were identical for both designs.

6. Influence of rotation on mechanical impedance estimation

When estimating mechanical load impedances, the method relies on detecting small changes in the measured transfer functions while assuming that these changes are caused only by variations in the attached translational mechanical impedance. If the rotational mechanical impedance is also changing, this will influence the torsional motion of the probe tip and in turn the measured velocity in z-direction. This may introduce an error in the estimation of the attached translational mechanical load impedance because the change in torsion cannot be measured with the measurement device.

Torsional motions of the probe tip are influenced by the rotational mechanical impedance of the measurement device, the rotational mechanical impedance of the attached load and the coupling between the load and the measurement device. The calibration loads are pure masses and thus their rotational mechanical impedances can be completely described by their mass [3, p.69].

In practice, the aim is to measure the translational mechanical impedance of human skin in vivo. Because of the elastin and collagen in the extracellular matrix of skin, the rotational and translational mechanical impedance of skin is also dependent on its stiffness and not only on its mass ([4], [5] ,[6]). The influence of the stiffness on the translational mechanical impedance can be measured with the measurement device. Since the torsion of the probe tip cannot be measured with the current measurement device, the influence of the stiffness on the torsion is unknown in the estimation process. An increase in rotational mechanical impedance of the attached load leads to a decrease in probe-tip motion. Since the underlying model assumes a linear relationship between the measured transfer function and the attached load, a decrease in motion will lead to an increase in the estimated translational mechanical load impedance, independent of whether the decrease resulted in a change in rotational mechanical impedance or translational mechanical impedance.
The largest error of this type is expected if torsional motion vanishes completely. For the estimation of this error, we use the relative error

$$\Delta H_{\mathrm{total,rot}} = \frac{H_{\mathrm{total}}}{H_{\mathrm{total}} - H_{\mathrm{rot}}}. \tag{11}$$

The result of this is shown in Figure 6 together with the transfer function level difference between a 6 mg pure mass and 13 mg pure mass as loads.
Figure 6 indicates that the influence of the torsional motion on the transfer function is small even compared to the small change in transfer function between the two smallest calibration loads 6 mg and 13 mg. In a second step we perform a calibration and use the model parameters to estimate the translational mechanical impedance of the calibration loads. Then, we subtract $\Delta H_{\mathrm{total,rot}}$ from the measured transfer functions for the different loads and calculate the translational mechanical impedance again. The level difference between both results can be seen as a maximum error due to torsional motions. The result of

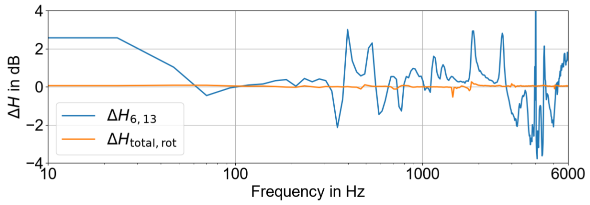

Figure 6: Measured difference in transfer function between 6 mg and 13 mg load (blue) together with the change in transfer function $\Delta H_{\text{total,rot}}$ of the unloaded case under the assumption that the torsional motion would vanish (orange).

this procedure is shown in Figure 7.

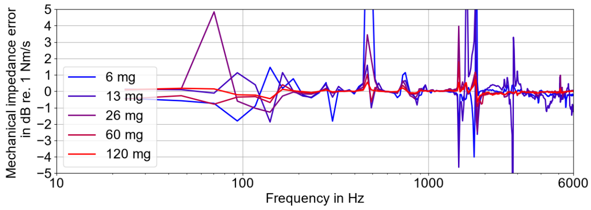

Figure 7: Change in estimated translational mechanical impedances for different load cases if the measured torsional components are removed from the measured transfer functions.

The largest errors can be seen for small translational mechanical impedances. With increasing mass, i.e. increasing mechanical impedance, a decrease in the error can be seen. For most frequencies and loads, the absolute error stays below 1 dB. The maximum error occurs at around 1800 Hz and is 15 dB in magnitude. This error reflects the extreme case that every torsional motion vanishes through an increase in rotational mechanical impedance in the attached load impedance or the coupling.

7. Discussion

The motivation to further investigate rotational motion in the measurement system originated in the very first prototype, which consisted only of a vibration exciter and an acceleration sensor. This design was more of a proof of concept of the calibration approach and rotational motions were not counteracted in any way. In order to make it applicable inside the ear canal, the exciter and acceleration sensor were placed on a cantilever beam. This paper aimed to investigate torsional motion in the measurement device and its influence on the estimation of attached mechanical load impedances.

FE simulations indicate no practically relevant contribution of rotational motions at low frequencies ($f < 1000$ Hz). However, at high frequencies ($f > 1000$ Hz), contributions from torsional motion appear to become closer to the overall translational velocity up to a point where the torsional contribution may become practically relevant. Also, slight displacements of the acceleration sensor up to half a millimeter, as would be realistic in a realistic environment, noticeably increased torsional motions. This is observable even for the smallest offset of 0.1 mm.

While simulations provide valuable insights into the mechanical behavior of systems, they are a simplification of physical processes. The exact material properties of the individual components of the measurement device (beam, piezo exciter and acceleration sensor) are not precisely known and therefore had to be estimated. In addition, the connections of the exciter and acceleration sensor to the beam were simplified by using a bonded contact/form union instead of the double-sided tape used in the physical prototype.

The experimental measurements confirmed the small influence of torsional motion at low frequencies. For high frequencies, the contribution of torsional motions was smaller than indicated by the simulations. The influence of torsional motion is small, even for the rectangular beam. The tuning-fork-shaped beam showed only a slightly larger mean level difference between translational and torsional motion than the rectangular beam. For the tuning-fork-shaped beam there are larger fluctuations in the level difference at high frequencies compared to the rectangular beam.

Finally, the influence of torsional motion, or more precisely of changes in torsional behavior, was investigated. When measuring on human skin, the torsional motion is expected to decrease relative to the calibration measurements. The error introduced by removing the torsional contribution was investigated and the measurements suggest that the largest resulting errors can be found for small mechanical load impedances. However, for most frequencies, the errors were below 1 dB for all chosen loads. The largest differences between including and neglecting torsional motion occurred in narrow-band frequency ranges. When comparing Figure 6 and 7, the error increased where the observed difference in the transfer functions approached zero. Here, even small changes/errors in the measured transfer functions can have a larger impact on the estimated mechanical load impedances. These results suggest that, although torsional motion occurs and is not included in the calibration model, its effect on estimation accuracy is small.

Although outside the scope of this paper, rotations about the x-axis due to bending waves may also constitute a source of error. Because the bending stiffness is lower than the torsional stiffness, rotations about the x-axis may involve larger rotation angles than torsional rotations about the y-axis. This should be further investigated in the future.

8. Summary

To investigate torsion at the tip of the measurement device and its influence on the estimation of attached load impedances, both simulations and measurements were conducted. The simulations indicated increasing amplitudes of torsional motion with increasing frequency. In contrast, the measurements showed that torsional motion remained relatively constant over frequency. While the simulations suggested a benefit of using a tuning-fork-shaped beam instead of a rectangular beam, the measurements showed that beam design had only a small effect on torsional motion at the probe tip. If changes in the coupling between the load and the measurement device, or an increased rotational mechanical impedance of the attached load, eliminated all torsional motion, the observed torsional contribution would lead to estimation errors below 1 dB for most frequencies. In narrow frequency bands, however, the errors exceeded 5 dB, with a maximum isolated peak of 15 dB at 1800 Hz.

References

[1] Benkert, M., Sankowsky-Rothe T., Kuipers, E., and Blau, M., "Development of a measurement system to determine human ear canal wall mechanical impedance in-situ: Method and sensitivity of early prototype," *DAS DAGA Conference Copenhagen*, 2025.

[2] Fahy, F. and Gardonio, P., *Sound and Structural Vibration.* Oxford, UK: Academic Press, 2007.

[3] A. Lenk, *Elektromechanische Systeme, Band 1: Systeme mit konzentrierten Parametern* (Elektromechanische Systeme), 3rd ed. Berlin: VEB Verlag Technik, 1971, vol. 1.

[4] Y. Nie, J. Wang, C. Zheng, *et al.*, "Measurement and modeling of the mechanical impedance of human mastoid and condyle," *The Journal of the Acoustical Society of America*, vol. 151, no. 3, pp. 1434–1448, Mar. 2022. DOI: 10.1121/10.0009618.

[5] T. Lei, L. Ye, Y. Pei, H. Sun, and C. Guo, "Applications of Elastin in Cosmetics: Prospects and Challenges," *Cosmetics*, vol. 12, no. 1, p. 18, Jan. 2025. DOI: 10.3390/cosmetics12010018.

[6] A. J. Heim, W. G. Matthews, and T. J. Koob, "Determination of the elastic modulus of native collagen fibrils via radial indentation," *Applied Physics Letters*, vol. 89, no. 18, p. 181 902, Oct. 2006. DOI: 10.1063/1.2367660.